

Nonlinear Magneto-Optics of Fe Monolayers from first principles: Structural dependence and spin-orbit coupling strength

J. P. Dewitz^{a,b}, Jian Chen^c, and W. Hübner^b

(a) *Institut für Theoretische Physik, Freie Universität Berlin, Arnimallee 14, D-14195 Berlin, Germany*

(b) *Max Planck Institut für Mikrostrukturphysik, Weinberg 2, D-06120 Halle/Saale, Germany*

(c) *Department of Physics, University of Florida, Gainesville, FL 32611, USA.*

(November 6, 2018)

Abstract

We calculate the nonlinear magneto-optical response of free-standing fcc (001), (110) and (111) oriented Fe monolayers. The bandstructures are determined from first principles using a full-potential LAPW method with the additional implementation of spin-orbit coupling. The variation of the spin-orbit coupling strength and the nonlinear magneto-optical spectra upon layer orientation are investigated. We find characteristic differences which indicate an enhanced sensitivity of nonlinear magneto-optics to surface orientation and variation of the in-plane lattice constants. In particular the crossover from onedimensional stripe structures to twodimensional films of (111) layers exhibits a clean signature in the nonlinear Kerr-spectra and demonstrates the versatility of nonlinear magneto-optics as a tool for *in situ* thin-film analysis.

75.30.Pd;78.20.Ls;73.20.At;75.50.Bb

I. INTRODUCTION

The Nonlinear Magneto-Optical Kerr effect (NOLIMOE) is a unique optical tool to analyze thin-film systems, since it is exclusively generated at surfaces and interfaces, where the local inversion symmetry is broken [1]. Therefore it has attracted considerable interest in recent research on interface magnetism [2–10]. In this paper we investigate the dependence of the nonlinear magneto-optical Kerr-spectra and their microscopic origin [11] – the spin-orbit coupling (SOC) and the magnetic moment – of Fe monolayers on structural changes. In particular the effects of different in-plane lattice constants, different coordination and onedimensional stripe structures are studied. The results were obtained using the full potential linearized augmented plane wave (FLAPW) method WIEN95 [12] with the additionally performed implementation of spin-orbit coupling.

Two features are responsible for the strong interest in magnetic thin films: (i) the magnetic properties strongly depend on structural changes and (ii) the spin-orbit induced effects like magnetic anisotropy and giant magnetoresistance (GMR) are much larger in low dimensional systems. Whereas the magnetic anisotropy is in general larger in twodimensional systems due to the reduced symmetry and thus a different crystal potential, the change of the magnetic moments is generated by the magneto-volume effect, i.e. the dependence of the magnetic moment on the atomic volume [13–16]. The latter is affected by the differences between the equilibrium lattice constants of substrate and overlayer and the induced overlayer structures. One of the most striking examples is the Fe/Cu(001) system which shows a rich magnetic phase diagram in the range from 1 to 11 monolayers [17–19]. Therein heavily distorted fcc structures appear. The interlayer distances are relaxed (resulting in a fct structure) and shifts of the atomic positions in and perpendicular to the layer plane occur [20]. Also the in-plane lattice constants of consecutive layers are relaxed. For the Fe/Cu(001) system experiments [6] confirmed the sensitivity of NOLIMOE on structural changes of the top layer.

Since all these effects take place in configurations with only a few monolayers it is possible to obtain them directly by *ab initio* methods. A lot of calculations were done for freestanding and supported monolayers, most of them aiming at the computation of magnetic anisotropy. For 3d transition metals the effects of hybridization with the substrate [21], different coordination and *d*-band filling [22,23], the stability of the monolayer for different magnetic configurations, such as ferromagnetic, antiferromagnetic or canted spin [24–26], and superstructures [27] were calculated from first principles.

Since the theoretical prediction of the sensitivity of nonlinear optics to surface magnetism [28–30] and the first experiments [2,3] the applicability of NOLIMOE to thin film systems has been demonstrated for several phenomena. Due to the fact that SHG is also generated at buried interfaces, properties of different interfaces in multilayer systems could be separated [31,32]. For that purpose it was important that the size of the nonlinear magneto-optical effects, namely the nonlinear Kerr rotation, is strongly increased compared to linear optics [33,34]. These measurements also show a dependence on interface roughness [35]. By direct comparison of linear and nonlinear MOKE, changes of the magnetic properties of the topmost layer during the growth process were detected for the Co/Cu(001) system [36], since NOLIMOE is sensitive to the surface and interlayer only while linear MOKE integrates over the magnetism of all layers. Also quantum well states which occur in

sandwich structures could be resolved. This has been shown both experimentally [9,37–39] and theoretically [7], by exploiting the fact that NOLIMOKE spectra reflect characteristic features of the bandstructures [40]. Recent work predicted that even the influence of surface antiferromagnetism on the optical signal can be resolved by the nonlinear magneto-optical Kerr-effect (NOLIMOKE) [8]. This has already been shown before for SHG of the antiferromagnetic non-inversion symmetric bulk Cr_2O_3 [41,42].

One further potential of SHG, which to our knowledge has not been applied to magnetic systems so far, is the strongly enhanced sensitivity to submonolayer coverages [43,44]. Second harmonic generation by small particles is enhanced by local-field effects. In the case of clusters deposited on a substrate this gives rise to signals for particle sizes around 1 nm [45], which is far beyond the resolution limit of linear optics. For spherical particles the effects of local-field enhancement are well known by the linear Mie theory [46]. Extensions to nonlinear optics [47] show an enhanced sensitivity of the size-dependent resonances compared to the linear case [48]. In the case of 3d transition-metal overlayers it should be possible to resolve nanostructures of nm size with low density by making use of the submonolayer coverage sensitivity of SHG and the different in-plane symmetries of the nanostructures and the substrate. From the experimental point of view the preparation of nanostructures can now be achieved by state of the art techniques such as molecular beam epitaxy varying the growth parameters (e.g. the deposition rate or the temperature [49,50]).

So far calculations of SHG generated by metal surfaces are mainly restricted to simple and noble metals which are well described by the model of a free electron gas. These systems were intensely studied by Liebsch and coworkers [51–53]. They also calculated anisotropic contributions [54–56] and the influence of steps [57–59] and obtain good agreement with experiment. Other authors studied the change of the SHG yield in the presence of adsorbates on simple metal surfaces within density functional theory [60–62]. For these nonmagnetic systems the intraband transitions show stronger contributions than the interband transition. Thus a better model for the screening effects is necessary, whereas in the case of transition metals the response is mainly due to interband transitions. Then the intraband effects can be added by applying a Drude model using experimental parameters [63]. Calculations of the linear magneto-optical Kerr-effect (MOKE) indicate that *ab initio* methods including spin-orbit coupling and an highly accurate determination of the dipole transition matrix elements are necessary to obtain magneto-optical spectra which can be compared to experimental values [63–65]. To some extent this was realized for nonlinear magneto-optics by Pustogowa *et al.* [66]. In their work the Kerr spectra of Fe films with one to seven layers and the dependence of the Kerr-spectra of a Fe(001) monolayer on the in-plane lattice constant have been calculated by determining the electronic bands within a full potential linear muffin tin orbital (FP-LMTO) code. Spin-orbit coupling was treated within first-order perturbation theory and the optical matrix elements were approximated as constants.

Here we will use the FLAPW method and go beyond this work within two respects: different orientations of Fe-monolayers ((001),(110),(111) of fcc) are investigated and, apart from the Kerr-spectra and the magnetic moments, we focus on the spin-orbit coupling strength and its structural dependence. Though microscopically both spin-orbit coupling and spin-polarization are necessary to generate magneto-optical response, spin-orbit coupling plays a special role, since the spin-orbit coupling strength is directly proportional to the size of the magneto-optical Kerr effect. This is known from studies of linear MOKE [67,68]. Thus e.g.

the Kerr-rotation of an Fe/Pt system is much larger than that of an Fe layer, since the large spin-orbit coupling of Pt contributes via hybridization with the magnetic Fe-layer [64,69]. This knowledge is important for applications in storage technology, where magneto-optics is applied in a configuration, where a perpendicular easy axis in combination with an increased Kerr-rotation is preferred. In contrast to the spin-orbit coupling the dependence on the magnetic moment is rather complicated. Nevertheless little is known about the spin-orbit coupling constants of thin film systems contrary to their magnetic moments.

In our work the optical spectra are determined by using the same approximations as in [66], i.e. the matrix elements are taken as constants and the effects of spin-orbit coupling in the wavefunctions are treated within first-order perturbation theory. Since the spin-orbit induced changes of the wavefunctions yield first-order effects [70] while spin-orbit induced shifts of the eigenenergies give rise to second-order effects, we neglect spin-orbit coupling in the calculations of the electronic bands, which are obtained from first principles. The validity of this approach will be shown below.

By the choice of the investigated monolayers, we want to study several aspects of structural changes. Firstly, we investigate the influence of relaxation of the in-plane lattice constant, which is varied over a wide range for the Fe(001) monolayer. Secondly, substrates of different orientations are simulated by comparing the results for the Fe(001), Fe(110) and Fe(111) monolayers, which also reveals the role of coordination. These structures are deduced from the bulk fcc lattice. Two lattice constants are considered, the lattice constant induced by Cu fcc bulk and an even smaller value. Thirdly, the role of nanostructuring is studied for regular arrays of stripes, which can be created by viewing the closed monolayer as a regular array of chains and then relaxing the distance between the chains. Although this structure is rather artificial, it reveals the effect of reducing the dimension of the layer in a second direction. Also we compare our results with previous calculations.

Future work will address the calculation of the optical dipole matrix elements to get the full information on the size of the NOLIMOKE spectra and to exploit the symmetry properties of the systems, which will be of special interest in the calculation of special nanostructures like triangular islands. This includes the determination of the lateral resolution limit of nonlinear optics.

The paper is organized as follows: In Sec. II, we will outline the theory for the nonlinear magneto-optical response and our method to calculate the spin-orbit coupling. Then the result part follows, which is divided into three subsections (Secs. III A, B, C), each for the comparison of different characteristic changes of the structures. The paper ends with summary and outlook (Sec. IV).

II. THEORY

Within the electric-dipole approximation the polarization \mathbf{P} of the medium can be expanded in terms of the incident field \mathbf{E} as

$$P_i = \chi_{ij}^{(1)} E_j + \chi_{ijk}^{(2)} E_j E_k + \dots ,$$

where $\chi^{(1)}$ and $\chi^{(2)}$ are the linear and second harmonic susceptibilities [1]. We calculate the nonlinear magneto-optical response within the theoretical framework introduced by Hübner and Bennemann [29] and obtain the nonlinear susceptibility in the electric dipole approximation as

$$\begin{aligned} \chi_{ijk}^{(2)}(2\mathbf{q}, 2\omega) = & \frac{-ie^3}{2q^3\Omega} \sum_{\mathbf{k}, l, l', l''} \left\{ \langle \mathbf{k} + 2\mathbf{q}, l'' | i | \mathbf{k}, l \rangle \langle \mathbf{k}, l | j | \mathbf{k} + \mathbf{q}, l' \rangle \langle \mathbf{k} + \mathbf{q}, l' | k | \mathbf{k} + 2\mathbf{q}, l'' \rangle \right. \\ & \left. \times \frac{f(E_{\mathbf{k}+2\mathbf{q}, l''}) - f(E_{\mathbf{k}+\mathbf{q}, l'})}{E_{\mathbf{k}+2\mathbf{q}, l''} - E_{\mathbf{k}+\mathbf{q}, l'} - \hbar\omega + i\hbar\alpha_1} - \frac{f(E_{\mathbf{k}+\mathbf{q}, l'}) - f(E_{\mathbf{k}, l})}{E_{\mathbf{k}+\mathbf{q}, l'} - E_{\mathbf{k}, l} - \hbar\omega + i\hbar\alpha_1} \right\} . \end{aligned} \quad (1)$$

The indices i, j, k run over x, y and z . In previous calculations [66] the wave-functions and the band energies were calculated neglecting spin-orbit coupling. Instead spin-orbit coupling was taken as a perturbation and the product of the three matrix elements were calculated using first order perturbation theory to yield

$$\frac{\lambda_{so}}{\hbar\omega} \langle \mathbf{k} + 2\mathbf{q}, l'' | i | \mathbf{k}, l \rangle \langle \mathbf{k}, l | j | \mathbf{k} + \mathbf{q}, l' \rangle \langle \mathbf{k} + \mathbf{q}, l' | k | \mathbf{k} + 2\mathbf{q}, l'' \rangle \quad (2)$$

where the wavefunctions and energies do not contain spin-orbit coupling and the spin-orbit coupling constant is taken from the atomic value of the spin-polarized d -bands. The matrix elements are approximated as constants. This approach includes explicit inversion symmetry breaking but makes it impossible to distinguish the different elements of the tensor χ_{ijk} . Nevertheless the resulting nonlinear susceptibility

$$\chi^{(2)}(2\mathbf{q}_{||}, 2\omega, \mathbf{M}) = \frac{C^3 e^3 \mathbf{q}_{||} a \lambda_{so}}{\Omega \hbar\omega} \sum_{\sigma} \sum_{\mathbf{k}, l, l', l''} \frac{\frac{f(E_{\mathbf{k}+2\mathbf{q}_{||}, l''\sigma}) - f(E_{\mathbf{k}+\mathbf{q}_{||}, l'\sigma})}{E_{\mathbf{k}+2\mathbf{q}_{||}, l''\sigma} - E_{\mathbf{k}+\mathbf{q}_{||}, l'\sigma} - \hbar\omega + i\hbar\alpha_1} - \frac{f(E_{\mathbf{k}+\mathbf{q}_{||}, l'\sigma}) - f(E_{\mathbf{k}, l\sigma})}{E_{\mathbf{k}+\mathbf{q}_{||}, l'\sigma} - E_{\mathbf{k}, l\sigma} - \hbar\omega + i\hbar\alpha_1}}{E_{\mathbf{k}+2\mathbf{q}_{||}, l''\sigma} - E_{\mathbf{k}l\sigma} - 2\hbar\omega + i2\hbar\alpha_1} , \quad (3)$$

reflects the spectral dependence of a magnetic tensor element, since spin-orbit coupling enters in first order. Nonmagnetic tensor elements (and all even order tensor elements) also consist of the zeroth order (and the corresponding higher even orders) in spin-orbit coupling. Thus they do not contribute to magneto-optics within first order and yield larger values. Due to our approximations we add in Eq. (3) a spin index σ , drop the indices which specify the tensor elements and add the factor C^3 originated by the approximate size of the matrix elements.

The susceptibility is exclusively built on interband transitions. We will use this approximation throughout this paper, since interband resonances dominate the optical response of

metallic systems. Thus in our case we will call the dependence of $\omega^2 \text{Im}\chi^{(2)}(\omega)$ on the photon energy NOLIMOKE “spectra”. For details we refer to [66].

Calculations including spin-orbit coupling will only affect the band-energies $E_{\mathbf{k}}$, because the factor λ_{so} describes the effect of SOC in the wavefunctions and the matrix elements, which are included in $\chi^{(2)}$ as constants C , are not calculated explicitly.

In this work the bandstructures are obtained from first principles using the full potential linear augmented plane wave (FLAPW) method WIEN95 [12]. Additionally we implemented spin-orbit coupling in a second variational step as described e.g. by [21,71,72]. After the self-consistent determination of the wavefunctions and eigenenergies (quantities which are obtained self-consistently without SOC are marked by a suffix “sc” in the following) the Hamiltonian matrix is determined including spin-orbit coupling

$$\sum_{ij} \left\langle \phi_{\mathbf{k}_i}^{\text{sc}} | H^{\text{sc}} + H_{\text{so}} | \phi_{\mathbf{k}_j}^{\text{sc}} \right\rangle = \sum_{ij} \epsilon(q) \rho_i(q) \left\langle \phi_{\mathbf{k}_i}^{\text{sc}} | \phi_{\mathbf{k}_j}^{\text{sc}} \right\rangle$$

to obtain the eigenfunctions

$$\psi(q) = \sum_n \rho_n(q) \phi_{\mathbf{k}_n} \quad q = 1, 2, \dots$$

and the corresponding eigenenergies $\epsilon(q)$ shifted by spin-orbit coupling (q is the index of the eigenenergies and $\rho_n(q)$ is the coefficient of the n -th basis-function in the q -th eigenfunction). Here, spin-orbit coupling is not calculated self consistently, especially the basis functions are not affected by SOC. The procedure is known to yield good agreement with exact results [73].

To determine the spin-orbit part of the Hamiltonian the basis functions of the FLAPW method have to be taken into account. The basis set consists of the standard basis functions

$$\phi_{\mathbf{k}_i} = \begin{cases} \sum_{lm} [A_{lm}(\mathbf{k}_i) u_l(r, E_l) + B_{lm}(\mathbf{k}_i) \dot{u}_l(r, E_l)] Y_{lm} & r < R_{\text{mt}} \\ \frac{1}{\sqrt{\omega}} e^{i\mathbf{k}_i \cdot \mathbf{r}} & r > R_{\text{mt}} \end{cases} \quad (4)$$

and the so called *local orbitals*, which are introduced to describe the low lying semi-core states [72,74]

$$\phi_{\mathbf{k}_i}^{\text{LO}} = \begin{cases} \sum_{lm} [A_{lm}(\mathbf{k}_i) u_l(r, E_l) + B_{lm}(\mathbf{k}_i) \dot{u}_l(r, E_l) + C_{lm}(\mathbf{k}_i) \hat{u}_l(r, E_2)] Y_{lm} & r < R_{\text{mt}} \\ 0 & r > R_{\text{mt}} \end{cases} \quad (5)$$

and are included for all l -values for which semi-core states appear (R_{mt} is the muffin tin radius). The radial functions are obtained from the Schrödinger equation

$$\left[-\frac{2}{r} \frac{\partial}{\partial r} - \frac{\partial^2}{\partial r^2} + \frac{l(l+1)}{r^2} + V^\sigma(r) \right] u_l^\sigma(r) = E_l^\sigma u_l^\sigma(r), \quad (6)$$

where the localization energies E_l^σ are chosen to be at the center of the band.

The spin-orbit operator

$$H_{\text{so}} = \frac{\alpha^2}{2} \mathbf{s} \cdot (\vec{\nabla} V \times \mathbf{p})$$

(α is the fine structure constant) is applied in the spherical approximation:

$$\vec{\nabla}V = \frac{\mathbf{r}}{r} \frac{\partial V}{\partial r}$$

$$\frac{\partial V}{\partial r} \equiv 0, \quad r > R_{\text{mt}},$$

since the gradient of the potential yield its largest contributions near the core, where the potential is almost spherical. This yields

$$H_{\text{so}} = \frac{\alpha^2}{2} \mathbf{s} \cdot (\mathbf{r} \times \mathbf{p}) \frac{1}{r} \frac{\partial V}{\partial r} = \frac{\alpha^2}{2} \mathbf{s} \cdot \mathbf{L} \frac{1}{r} \frac{\partial V}{\partial r}.$$

The spin-orbit matrix elements

$$\langle \phi_{\mathbf{k}_i}^{\text{sc}} | H_{\text{so}} | \phi_{\mathbf{k}_j}^{\text{sc}} \rangle = \int_{r < R_{\text{mt}}} d\mathbf{r} \phi_{\mathbf{k}_i}^{\text{sc}*} \left(\frac{\alpha^2}{2} \mathbf{s} \cdot \mathbf{L} \frac{1}{r} \frac{\partial V}{\partial r} \right) \phi_{\mathbf{k}_j}^{\text{sc}} \quad (7)$$

$$\left(\int_{r > R_{\text{mt}}} d\mathbf{r} \phi_{\mathbf{k}_i}^{\text{sc}*} H_{\text{so}} \phi_{\mathbf{k}_j}^{\text{sc}} \equiv 0 \right)$$

are calculated by separating the angular and radial parts. This yields

$$\begin{aligned} &= \sum_{lmm'} \{ \lambda_{uu}^l A_{lm}^*(\mathbf{k}_i) A_{lm'}(\mathbf{k}_j) + \\ &\quad \lambda_{\dot{u}\dot{u}}^l B_{lm}^*(\mathbf{k}_i) B_{lm'}(\mathbf{k}_j) + \\ &\quad \lambda_{u\dot{u}}^l [A_{lm}^*(\mathbf{k}_i) B_{lm'}(\mathbf{k}_j) + B_{lm}^*(\mathbf{k}_i) A_{lm'}(\mathbf{k}_j)] \} \\ &\quad \cdot \left\langle \sigma \left| \int d\Omega Y_{lm}^*(\hat{r}) \mathbf{s} \cdot \mathbf{L} Y_{lm'}(\hat{r}) \right| \sigma' \right\rangle \end{aligned}$$

with the spin-orbit coupling constants

$$\begin{aligned} \lambda_{uu}^l &\equiv \frac{\alpha^2}{2} \int_{r < R_{\text{mt}}} dr u_l^\sigma(r) r \frac{\partial V_{\sigma'}}{\partial r} u_l^{\sigma'}(r) \\ \lambda_{u\dot{u}}^l &\equiv \frac{\alpha^2}{2} \int_{r < R_{\text{mt}}} dr u_l^\sigma(r) r \frac{\partial V_{\sigma'}}{\partial r} \dot{u}_l^{\sigma'}(r) \\ \lambda_{\dot{u}\dot{u}}^l &\equiv \frac{\alpha^2}{2} \int_{r < R_{\text{mt}}} dr \dot{u}_l^\sigma(r) r \frac{\partial V_{\sigma'}}{\partial r} \dot{u}_l^{\sigma'}(r) \end{aligned} \quad (8)$$

and the spin-orbit coupling constants including local orbital functions:

$$\begin{aligned} \lambda_{\dot{u}\hat{u}}^l &\equiv \frac{\alpha^2}{2} \int_{r < R_{\text{mt}}} dr \hat{u}_l^\sigma(r) r \frac{\partial V_{\sigma'}}{\partial r} \hat{u}_l^{\sigma'}(r) \\ \lambda_{\hat{u}u}^l &\equiv \frac{\alpha^2}{2} \int_{r < R_{\text{mt}}} dr \hat{u}_l^\sigma(r) r \frac{\partial V_{\sigma'}}{\partial r} u_l^{\sigma'}(r) \\ \lambda_{\hat{u}\dot{u}}^l &\equiv \frac{\alpha^2}{2} \int_{r < R_{\text{mt}}} dr \hat{u}_l^\sigma(r) r \frac{\partial V_{\sigma'}}{\partial r} \dot{u}_l^{\sigma'}(r) \end{aligned} \quad (9)$$

Thus we get three (six when local orbitals are involved) spin-orbit coupling constants for one l -value which are formed by a radial integral over the radial part of the basis functions and

the radial derivative of the potential. Furthermore one has to take into account that spin-orbit coupling mixes the spins, thus the Hamilton-matrix gets off-diagonal elements within the space of the spin \uparrow and \downarrow basis functions. Spin is not a good quantum number anymore and the wavefunctions consist of both spin \uparrow and spin \downarrow contributions. The spin-orbit matrix elements Eq. (7) get then additional spin indices σ and σ' .

$$\left\langle \phi_{\mathbf{k}_i, \sigma}^{\text{sc}} | H_{\text{so}} | \phi_{\mathbf{k}_j, \sigma'}^{\text{sc}} \right\rangle = \int_{r < R_{\text{mt}}} d\mathbf{r} \phi_{\mathbf{k}_i, \sigma}^{\text{sc}*} \left(\frac{\alpha^2}{2} \mathbf{s} \cdot \mathbf{L} \frac{1}{r} \frac{\partial V_{\sigma'}}{\partial r} \right) \phi_{\mathbf{k}_j, \sigma'}^{\text{sc}} \quad (10)$$

Therein the spin-index of the potential is equal to the spin index of the basis function on the right, since the spin-orbit operator acts on it. The fact that the potentials are different for the spins, but the basis functions are not, leads to the requirement to make the matrix explicitly hermitian, since the spin-orbit operator is. This affects only the spin-flip matrix elements.

III. RESULTS

In Sec. III. A we will simulate the effect of lattice relaxation. This can be achieved experimentally by different substrates, assuming pseudomorphic growth. We will show NOLIMOKE spectra of free-standing Fe(001) monolayers with in-plane lattice constants varied from $a = 2.4 \text{ \AA}$, which is slightly below the value of the nearest-neighbor distance in Cu fcc bulk $a=2.56 \text{ \AA}$, to $a = 2.76 \text{ \AA}$, which is close to the nearest-neighbor distance of Fe bcc bulk. For the comparison of the trends of the magnetic moments and the spin-orbit coupling constants we extend the range of lattice constants from 2.22 \AA to 3.18 \AA , the latter corresponding approximately to the value of bcc W. In Sec. III.B the same quantities are shown for Fe monolayers with different structures, i.e. the fcc (111), (001) and (110), which are schematically displayed in Fig. 1. The structures are studied for the Cu fcc nearest-neighbor distance $a=2.56 \text{ \AA}$ and $a = 2.4 \text{ \AA}$. It should be possible to get a measure of the structural changes from the NOLIMOKE spectra. In Sec. III.C we will show the influence of nanostructuring on the NOLIMOKE spectra by analyzing stripe structures as indicated in Fig. 2. The Fe(111) monolayer can be interpreted as an array of “zig-zag”-stripes. To reduce the dimension of the structure we vary the distance of the stripes, which is indicated by d , where in the case of $d = h$ the layer is equal to the (111) structure.

A. Fe(001) monolayers

Fig. 3 shows the NOLIMOKE spectra $\omega^2 \text{Im}\chi^{(2)}(\omega)$ of the Fe(001) monolayer as a function on the in-plane lattice constant. As analyzed by Pustogowa *et al.* [75] within a tight binding scheme the first maximum and the zero are mainly due to features of the d bands, whereas for higher photon energies the role of the $s-p$ -bands is more dominant. In particular they showed that the position of the zero is a measure for the d -band width and the height of the maximum is proportional to the magnetic moment. Thus the d bands generate the features of the spectra in the optical region. In our case the zeros show a clear dependence on the lattice constant. The positions shift to lower energies with increasing lattice constant. Since this point characterizes the d -bandwidth, the bandwidth is reduced upon lattice expansion. From the bandstructure it can also be seen that bands above the range of visible frequencies are shifted to lower energies with increasing lattice constant, which generates the different slopes in the high-energy part of the spectra. The height of the maxima starts to increase with the spin-polarization for lattice constants from 2.4 \AA to 2.58 \AA . For the larger lattice constants ($a=2.67$ and 2.76 \AA) there are no more significant changes of the peak height, as can be seen in the inset of Fig. 3. However, the position of the peaks is shifted in proportion to the value of the magnetic moments to lower energy values. The dependence of the maximum on the magnetic moments agrees with previous works [67,68], where no clear dependence of the linear magneto-optical response on the size of the magnetic moments was found. Additionally, from a tight binding calculation, Pustogowa *et al.* [75] found a linear dependence of the maximum for magnetic moments between 0 and $2.5 \mu_B$, but a similar behavior for moments between $2.5 \mu_B$ and $3.4 \mu_B$. The difference should reflect that in both calculations the magnetic moments are changed by different mechanisms. Whereas in the tight binding calculations the magnetic moments were affected by changes of the exchange coupling constant J , in our case the magnetic moments are varied by changing the lattice

constant, which does not only shift the relative positions of the d subbands, but also their width.

The values of the magnetic moments increase with increasing lattice constant. This is shown in Fig. 4, where the size of the magnetic moments (filled circles) is plotted as a function of the in-plane lattice constant in units of μ_B . If interpolated our results agree very well with calculations by Wang *et al.* [76], who obtained $3.04\mu_B$ for a lattice constant of $a = 2.56$ Å, and with results by Gay and Richter [77], who obtained $3.20\mu_B$ for a lattice constant of $a = 2.88$ Å compared to our results of $3.08\mu_B$ for $a = 2.56$ Å and $3.24\mu_B$ for $a = 2.88$ Å, respectively. Nevertheless one has to keep in mind that the error in the magnetic moments is around $\pm 5\%$ due to the chosen accuracy in our calculations.

In Fig. 4 we also compare the values of the magnetic moments directly with the spin-orbit coupling constants $\lambda_{uu}^{l=2}\uparrow\uparrow$ and $\lambda_{uu}^{l=2}\downarrow\downarrow$ defined in Eq. (8), i.e. the spin-orbit coupling constants for bands with d character for \uparrow and \downarrow spin. These constants are the important ones for magneto-optics since the d -bands exhibit the magnetic moments. Combinations of the radial functions other than (u_l, u_l) are of less interest since the radial dependence of wavefunctions is mainly described by the u_l -functions. The plot shows two important properties of the coupling constants: (i) The values increase with decreasing lattice constants and (ii) the difference between the coupling constants of \uparrow and \downarrow spin show a clear dependence on the magnetic moments. Inspection of the potentials for the different lattice constants shows that the size of the spin-orbit coupling constants is not directly governed by changes of the potential, i.e. the derivative of the potential shows no changes near the core, where the largest values of the derivative occur. As a consequence, the changes of the constants must be induced by changes of the radial functions. This is shown in Fig. 5, where the square of the function $u_l(r)$ and the integrand $u_l dV/dr u_l$ defined in Eq. (8) are plotted as a function of the radial distance. The insets show that the increase of the maximum of the integrand, which causes the changes of the coupling constants with decreasing lattice constants, is proportional to the changes of the square of u_l (the maxima of both quantities are normalized to one). Thus the changes of the coupling constants are caused by changes of the potential near the muffin tin radius R_{mt} , which alters the probability of the maximum of the radial functions also close to the nuclei. In addition the dependence of the differences between the $\uparrow\uparrow$ and $\downarrow\downarrow$ coupling constants on the magnetic moments reveals the variation of the potential with different spin-subband occupation and by changing the radial functions via Eq. (6). For even larger values of the lattice constants the coupling constants should reach the atomic value, which is approximately 50 meV. In the case of Ge, the spin-orbit splitting of the $4p$ electrons in the solid is 0.43 eV [78] at the Γ point, a 30% enhancement to the spin-orbit splitting of 0.21 eV in the Ge atom. By comparing the wavefunctions and potentials in the solid and the atom, we find that this increase in the spin-orbit coupling strength in the solid in Ge is caused by a quite different reason. Because of the covalent bond the charge distribution is not only enhanced between the atoms but also near the core. Daalderop *et al.* [71] obtained the coupling constants of bulk Fe and find a much larger difference between the coupling constants for \uparrow and \downarrow spin and also the values differ slightly. Since they used a LMTO code the differences should mainly be due to the different definitions of the coupling constants resulting from the different basis sets used.

In Tab. I the values of the additional spin-orbit coupling constants for $l = 1$ and 2 and within the combinations of the radial functions (u_l, u_l) and (\dot{u}_l, \dot{u}_l) are listed. The dependence

of the coupling constants λ_{uu}^l with $l = 1$ on the lattice constant differs significantly from the values for $l = 2$. Their changes are much more pronounced, namely the values decrease by about 40% rather than by only 5% for $l = 2$. Also a spin-polarization appears only for the largest value of the lattice constants whereas it slightly changes for $l = 2$. These properties reveal that the p states are much more influenced by the changed binding characteristics. Though in the case of Fe monolayers the p band is not occupied and its center is tens of eV above the Fermi-level, p -states could become accessible by optical excitations via hybridization with low lying s - and p -bands of an appropriate substrate such as Mo or W. In these systems the large values of the SOC-constants could, in particular in the case of pump-probe femtosecond spin dynamic experiments, significantly affect spin-orbit induced spin-flip contributions by strong excitations.

In principle contributions related to the radial functions \dot{u}_l should not contribute significantly since the values of the coefficients B_{lm} are in general much smaller than A_{lm} , nevertheless the changes of the coupling constants λ_{uu}^l should reflect some features of the shape of the bands. Since the values for $l = 2$ show no spin-polarization, the shape of the subbands should be nearly equal, also the derivative increases quite strongly with the lattice constants indicating narrower bands. For $l = 1$ the increase is even stronger in agreement with the values for $\lambda_{uu}^{l=1}$, the smaller values compared to $l = 2$ reflect stronger dispersed bands.

A direct comparison of the spectra of the Fe(001) monolayer for $a = 2.76$ Å obtained within the FLMTO method [79] and our FLAPW method in Fig. 6 shows good agreement in the region of low photon energies. The position of the maximum is near 1.5 eV in both cases and the energy where the susceptibility crosses zero is 3 eV. In both calculations the same model for the nonlinear magneto-optical susceptibility was applied. Thus the differences in the region of higher photon energies should be an effect of the different *ab initio* methods and in this special case due to the different basis sets. In the LMTO-method the number of basis functions is much smaller than in the FLAPW method which leads to a lack of bands high above the Fermi-level unless the calculations are performed for several localization energies. This is in agreement with the fact that for spectra which are based on the Fe bulk bandstructure we find no significant differences in both methods also for high photon energies.

Our results obtained for the changed lattice constants agree very well with the results by Pustogowa *et al.* [66] for the same system. Since they calculated spectra for lattice constants larger than 2.76 Å their changes of the zero are smaller due to the nonlinear dependence of the shape of the bands on the lattice constants, which is also reflected by the dependence of the magnetic moments on the lattice constants in Fig. 4. In contrast to their calculations in our case the position of the maximum shows a clear dependence on the lattice constant.

The optical spectra also depend on the type of approximations applied to the calculations of the electronic bands. This can be seen in Fig. 7, where the spectrum of a Fe(001) monolayer with $a = 2.76$ Å is calculated using different approximations for the exchange correlation potential. We compare the generalized gradient approximation (GGA), which is used for all calculations throughout this work, in the parameterization by Perdew *et al.* [80] with the local spin density approximation (LSDA) in the parameterization of Perdew and Wang [81]. Since GGA corrects for overbinding, the bandwidth should be lowered and thus the zero should be at lower energy. In our case the opposite behavior occurs. The LSDA

values are lower in energy. The spectra obtained with the different LSDA approximations show no strong deviations. GGA yields a slightly higher magnetic moment which can be responsible for the higher value of the maximum and the larger value of the zero. In general it is expected that spin-orbit coupling counteracts GGA, since the bandwidth increases by spin-orbit induced shifts. But in the case of the NOLIMOKE spectra the effects of spin-orbit coupling which enters the spectra via the bandstructure are negligible as can be seen in Fig. 8, where the NOLIMOKE spectrum of Fe(110) is plotted both with and without SOC effects on the bandstructure. This reflects that spin-orbit induced changes of the eigenenergies only contribute in second order to the spectrum [70].

B. Fe(001), (110) und (111) monolayers

In Figs. 9 and 10 the NOLIMOKE spectra of the Fe(001), (110) and (111) monolayers are compared for the nearest-neighbor distance of Cu fcc bulk, $a=2.56$ Å, and for $a=2.4$ Å. Since the nearest-neighbor distance is equal in the different structures, the changes reveal the different coordination, which is six in the hexagonal (111) layer, four in the square lattice (001) and two in the rectangular lattice (110). The different coordination determines the area of the twodimensional (see Fig. 1) unit cell containing one atom to $\sqrt{2}a^2$ for the (110) structure, a^2 for (001) and $\sqrt{3}/2a^2$ for (111). The next nearest neighbor distance is $\sqrt{2}a$ in the (110), $2a$ in the (001) and $\sqrt{3}a$ in the (111) layer.

For both nearest-neighbor distances it can be seen that the lattice with the lowest coordination shows the smoothest spectra, whereas for highest coordination the most complicated structure appears. This is a general aspect of coordination and can also be seen in the bandstructures [82]. Between 0 eV and the zero around 3 to 4 eV the (110) spectrum has a sinusoidal shape, in the (001) spectra first a maximum followed by a shoulder appears, whereas in the (111) case a dominant maximum is surrounded by two shoulders. The differences are much more pronounced for the smaller nearest-neighbor distance, in the case of $a=2.56$ Å the spectra are closer, as can be seen e.g. at the zero point, and it is more difficult to define a maximum. Comparing the positions of the zero for both lattice constants one notices that the shifts are larger for higher coordination. Whereas the zero remains more or less constant in the case of Fe(110), it is shifted to lower energies by approx. 0.2 eV for Fe(001) and 0.4 eV for Fe(111). Thus one can say that the dependence of the spectra on the lattice constants is proportional to the coordination.

Roughly the same holds for the magnetic moments in Figs. 11 and 12. There the magnetic moments and the spin-orbit coupling constants $\lambda_{uu}^{l=2} \uparrow\uparrow$ and $\lambda_{uu}^{l=2} \downarrow\downarrow$ are plotted for three different coordination numbers corresponding to (111), (001) and (110) layers. The magnetic moments of the Fe(110) layers change by only approx. 0.1 μ_B compared to approx. 0.25 μ_B for the (111) and (001) monolayers. As expected the values of the magnetic moments increase with lowered coordination. Comparison of the spin-orbit coupling constants show that the changes induced by the different coordination are quite small compared to the changes induced by different nearest-neighbor distances. Thus one can say that in a first approximation the values of the spin-orbit coupling constants depend on the nearest-neighbor distance and remain constant for different coordination. The values of the coupling constants with $l = 1$ and the combination of the radial functions (u_l, u_l) confirm this since they show no significant changes with the coordination as can be seen from Tabs. II and III.

C. Stripe structures

The NOLIMOKE spectra of the stripe structures of Fig. 2 are plotted in Fig. 13 for different distances d of the stripes in comparison to the spectrum of the Fe(111) monolayer, which can be interpreted as a stripe structure with distance $d = h$ (see Fig. 2). The spectra show no behavior which can be easily interpreted in terms of the bandwidth, corresponding to a zero point in the spectra, or the magnetic moment, corresponding to a maximum at a certain position in the low-energy-regime. Only the more complicated structure of the spectra for $d > h$ is clear from the lifting of degeneracies in the bandstructure, which results from the breaking of symmetry. Thus, the number of bands increases for $d > h$, since there are two nonequivalent atoms in the unit cell, compared to one for Fe(111). Since the bandstructures of the different stripe structures show no pronounced overall changes, the differences in the spectra should be an effect of the details of the bands.

If one first neglects the spectra for the stripes with the largest distance (long-dashed line) the behavior is quite regular in the sense that the maximum value of the spectra decreases with increasing distance and that the zero point shifts to lower energies and reaches zero for $d = h + 1.04 \text{ \AA}$. By drastically increasing the “interstripe” distance to $d = h + 1.78 \text{ \AA}$ the NOLIMOKE spectra differ from these trends and exhibit a shape which is similar to the spectra of the closed layers in Fig. 3, 9 and 10. This can be interpreted as an oscillatory behavior of the electronic structure with the distance. The change of the trends for the distance of $d = h + 1.78 \text{ \AA}$ can also be observed in Fig. 14 for the spin-orbit coupling constants and more or less also for the magnetic moments. Since the difference of their values for $d = h + 1.04 \text{ \AA}$ and $d = h + 1.78 \text{ \AA}$ is very small, μ remains essentially constant.

The relatively small changes of the spin-orbit coupling constants with $l = 2$ shown in Fig. 14 and Tab. IV imply the same interpretation as in Sec. III.B for the layers with different coordination. In a first approximation the values of the coupling constants remain unchanged and thus their values depend mainly on the nearest-neighbor distance, which is fixed here by the constant structure of the isolated stripes. Thus, for tailoring the SOC-constants and the magnetic moments, the choice of the substrate will be much more efficient than nanostructuring while keeping the nearest-neighbor distance constant. Nevertheless nanostructuring can still have a strong effect on dynamical properties of the spin and magnetic moments, for which the size of the SOC-constants is quite important. For certain island sizes a phase transition from ferro- to superparagnetism will occur and affect the spin dynamics.

The behavior of the coupling constants with $l = 1$, which are also listed in Tab. IV, show one difference. The values are also nearly constant for distances larger than h , but they show a clear increase, when the distance changes from $d = h$ to $d = h + 0.46 \text{ \AA}$, i.e. at the onset of the reduction of the symmetry. Thus the SOC-constants of the p -bands are not only much larger but also much more sensitive to the bond characteristics than the d -bands.

Clearly further investigations are necessary to understand the strong changes of the NOLIMOKE spectra for the different stripe distances.

IV. SUMMARY AND OUTLOOK

We presented results for the structural dependence of the nonlinear magneto-optics of Fe monolayers. Since in our theory the optical dipole-transition matrix elements are approximated as constants, we cannot analyze the symmetry properties of the nonlinear susceptibility tensor. Instead we focused on the spectral dependence of a magnetic tensor element, the magnetic moments, and the spin-orbit coupling constants, the latter two reflecting the microscopic origin of magneto-optics.

In the case of the Fe(001) monolayer-spectrum the characteristic features like the position of the first zero, which is related to the d -band width, and the position of the maxima are shifted to lower energies with decreasing lattice constant. The changes are stronger for smaller lattice constants, which also holds for the magnetic moments and the spin-orbit coupling constants. The values of the maxima, which should be related to the magnetic moments show no clear trend. The spectra of layers with different coordination numbers show characteristic differences in the shape as well as in the position of the maximum and the first zero. The differences are more pronounced for smaller lattice constants. Reducing the dimensionality of the monolayers, simulated by onedimensional stripes with different “interstripe”-distances, results in dramatic changes of the spectra. Their shapes show no similarities with the monolayer spectra any more. In contrast the values of the spin-orbit coupling constants depend in a first approximation only on the nearest-neighbor distance. This was shown for both the Fe monolayers with different coordination number and the onedimensional stripe structures.

For the Fe(001) monolayers the SOC-constants show the opposite behavior as the magnetic moments, they increase with decreasing lattice constants. As an important result the difference between the coupling constants for \uparrow and \downarrow spin is proportional to the magnetic moments, caused by the dependence of the potentials on the occupation of the subbands. The values of the magnetic moments show results well-known for itinerant ferromagnets. Increasing the lattice constants or decreasing the coordination enhances their values. The same holds for increasing the distances of stripes in the quasi-onedimensional structures.

Our results clearly show the strong dependence of the NOLIMOKE spectra on structural changes and also indicate that the spectral dependence of the magneto-optical response is a valuable source of information on the structure of the investigated system.

Future work will address the completion of our *ab initio* theory by the optical transition dipole matrix elements, which is of major importance not only for the determination of absolute signal values but also for the study of structural dependencies, since the susceptibility tensor reflects the symmetry of the system. Also we will investigate structures with further reduced dimensionality, i.e. zerodimensional islands, and apply nonlinear magneto-optics to antiferromagnets.

We acknowledge financial support by Deutsche Forschungsgemeinschaft through Sfb 290 and by TMR Network NOMOKE contract No. FMRX-CT96-0015.

REFERENCES

- [1] Y. R. Shen, *The principles of nonlinear optics*, Wiley, New York (1984).
- [2] J. Reif, J. C. Zink, C.-M. Schneider, and J. Kirschner, Phys. Rev. Lett. **67**, 2878 (1991).
- [3] J. Reif, C. Rau, and E. Matthias, Phys. Rev. Lett. **71**, 1931 (1993).
- [4] H. A. Wierenga, W. de Jong, M. W. J. Prins, Th. Rasing, R. Vollmer, H. Schwabe, and J. Kirschner, Phys. Rev. Lett. **74**, 1462 (1995).
- [5] B. Koopmanns, M. G. Koerkamp, Th. Rasing, and H. van den Berg, Phys. Rev. Lett. **74**, 3692 (1995).
- [6] M. Straub, R. Vollmer, and J. Kirschner, Phys. Rev. Lett. **77**, 743 (1996).
- [7] T. A. Luce, W. Hübner, and K. H. Bennemann, Phys. Rev. Lett. **77**, 2810 (1996).
- [8] A. Dähn, W. Hübner, and K. H. Bennemann, Phys. Rev. Lett. **77**, 3929 (1996).
- [9] A. Kirilyuk, Th. Rasing, R. Mégy, and P. Beauvillain, Phys. Rev. Lett. **77**, 4608 (1996).
- [10] V. V. Pavlov, R. V. Pisarev, A. Kirilyuk, and Th. Rasing, Phys. Rev. Lett. **78**, 2004 (1997).
- [11] P. N. Argyres, Phys. Rev. **97**, 334 (1955).
- [12] P. Blaha, K. Schwarz, P. Dufek, and R. Augustyn, WIEN95, Technical University of Vienna 1995. (Improved and updated Unix version of the original copyrighted WIEN-code, which was published by P. Blaha, K. Schwarz, P. Sorantin, and S. B. Trickey, in Comput. Phys. Commun. **59**, 399 (1990)).
- [13] C. S. Wang, B. M. Klein, and H. Krakauer, Phys. Rev. Lett. **54**, 1852 (1985).
- [14] P. M. Marcus and J. Kübler, Phys. Rev. B **39**, 6957 (1989).
- [15] V. L. Moruzzi, P. M. Marcus, K. Schwarz, and P. Mohn, Phys. Rev. B **34**, 1784 (1986).
- [16] F. J. Pinski, J. Staunton, B. L. Gyorffy, D. D. Johnson, and G. M. Stocks, Phys. Rev. Lett. **56**, 2096 (1986).
- [17] W. Daum, C. Stuhlmann, and H. Ibach, Phys. Rev. Lett. **60**, 2741 (1988).
- [18] J. Giergiel, J. Kirschner, J. Landgraf, J. Shen, and J. Woltersdorf, Surf Sci. **310**, 1 (1994).
- [19] M. Zharnikov, A. Dittschar, W. Kuch, C. M. Schneider, and J. Kirschner, Phys. Rev. Lett. **76**, 4620 (1996).
- [20] S. Müller, P. Bayer, C. Reischl, K. Heinz, B. Feldmann, H. Zillgen, and M. Wuttig, Phys. Rev. Lett. **74**, 765 (1995).
- [21] Chun Li, A. J. Freeman, H. J. F. Jansen, and C. L. Fu, Phys. Rev. B **42**, 5433 (1990).
- [22] E. Wimmer, J. Phys. F: Met. Phys. **14**, 2613 (1984).
- [23] S. Blügel, M. Weinert, and P. H. Dederichs, Phys. Rev. Lett. **60**, 1077 (1988).
- [24] S. Blügel, B. Drittler, R. Zeller, and P. H. Dederichs, Appl. Phys. A **49**, 547 (1989).
- [25] R. Pentcheva, Dipl. thesis, Jülich 1997.
- [26] R. Lorenz and J. Hafner, Phys. Rev. B **54**, 15937 (1996).
- [27] L. Nordström and D. J. Singh, J. Vac. Sci. Technol. B **14**, 3160 (1996).
- [28] Ru-Pin Pan, H. D. Wei, and Y. R. Shen, Phys. Rev. B **39**, 1229 (1989).
- [29] W. Hübner and K. H. Bennemann, Phys. Rev. B **40**, 5973 (1989).
- [30] W. Hübner, Phys. Rev. B **42**, 11553 (1990).
- [31] M. G. Koerkamp and T. Rasing, Surf. Sci. **352-354**, 933 (1996).
- [32] H. A. Wierenga, W. de Jong, M. W. J. Pirns, Th. Rasing, R. Vollmer, A. Kirilyuk, H. Schwabe, and J. Kirschner, Surf. Sci. **331-333**, 1294 (1995).
- [33] U. Pustogowa, W. Hübner, and K. H. Bennemann, Phys. Rev. B **49**, 10031 (1994).

[34] U. Pustogowa, W. Hübner, and K. H. Bennemann, *J. Magn. Magn. Mat.* **148**, 269 (1995).

[35] M. Groot Koerkamp, and T. Rasing, *J. Magn. Magn. Mater.* **156**, 213 (1996).

[36] R. Vollmer, A. Kirilyuk, H. Schwabe, J. Kirschner, H. A. Wierenga, W. de Jong, and T. Rasing, *J. Magn. Magn. Mater.* **148**, 295 (1995).

[37] M. Straub, R. Vollmer, and J. Kirschner, *Verh. Dtsch. Phys. Ges.* **6**, 1595 (1996).

[38] M. Straub, R. Vollmer, and J. Kirschner, *Verh. Dtsch. Phys. Ges.* **7**, 818 (1997).

[39] P. van Gelderen, S. Crampin, T. Rasing, and J. E. Inglesfield, *Phys. Rev. B* **54**, R2343 (1996).

[40] U. Pustogowa, W. Hübner, and K. H. Bennemann, *Phys. Rev. B* **48**, 8607 (1993).

[41] M. Fiebig, D. Fröhlich, B. B. Krichevtskov, and R. V. Pisarev, *Phys. Rev. Lett.* **73**, 2127 (1994).

[42] V. N. Muthukumar, R. Valenti, and C. Gros, *Phys. Rev. Lett.* **75**, 2766 (1995).

[43] Y. R. Shen, *Ann. Rev. Mater. Sci.* **16**, 69 (1986).

[44] G. L. Richmond, J. M. Robinson, and V. L. Shannon, *Prog. Surf. Sci.* **28**, 1 (1988).

[45] T. Götz, F. Träger, M. Buck, C. Dressler, and F. Eisert, *Appl. Phys. A* **60**, 607 (1995).

[46] G. Mie, *Ann. Phys.* **25**, 377 (1908).

[47] D. Östling, P. Stampfli, and K. H. Bennemann, *Z. Phys. D* **28**, 169 (1993).

[48] J. P. Dewitz, W. Hübner, and K. H. Bennemann, *Z. Phys. D* **37**, 75 (1996).

[49] H. Röder, E. Hahn, H. Brune, J.-P. Bucher, and K. Kern, *Nature* **366**, 141 (1993).

[50] H. Brune, C. Romainczyk, H. Röder, and K. Kern, *Nature* **369**, 469 (1993).

[51] A. Liebsch, *Phys. Rev. Lett.* **61**, 1233 (1988).

[52] M. Weber and A. Liebsch, *Phys. Rev. B* **35**, 7411 (1987).

[53] M. G. Weber and A. Liebsch, *Phys. Rev. B* **36**, 6411 (1987).

[54] A. V. Petukhov and A. Liebsch, *Surf. Sci.* **320**, L51 (1994).

[55] A. V. Petukhov and A. Liebsch, *Surf. Sci.* **331-333**, 1335 (1995).

[56] A. V. Petukhov and A. Liebsch, *Surf. Sci.* **334**, 195 (1995).

[57] H. Ishida and A. Liebsch, *Phys. Rev. B* **46**, 7153 (1992).

[58] H. Ishida and A. Liebsch, *Surf. Sci.* **297**, 106 (1993).

[59] H. Ishida and A. Liebsch, *Phys. Rev. B* **50**, 4834 (1994).

[60] M. Kuchler and F. Rebentrost, *Phys. Rev. Lett.* **71**, 2662 (1993).

[61] M. Kuchler and F. Rebentrost, *Phys. Rev. B* **50**, 5651 (1994).

[62] F. Rebentrost, *Prog. Surf. Sci.* **48**, 71 (1995).

[63] P. M. Oppeneer, T. Maurer, J. Sticht, and J. Kübler, *Phys. Rev. B* **45**, 10924 (1992).

[64] G. Y. Guo and H. Ebert, *Phys. Rev. B* **51**, 12633 (1995).

[65] H. Ebert, *Rep. Prog. Phys.* **59**, 1665 (1996).

[66] U. Pustogowa, W. Hübner, K. H. Bennemann, and T. Kraft, *Z. Phys. B* **102**, 109 (1997).

[67] P. M. Oppeneer, J. Sticht, T. Maurer, and J. Kübler, *Z. Phys. B* **88**, 309 (1992).

[68] D. K. Misemer, *J. Magn. Magn. Mater.* **72**, 267 (1988).

[69] H. Ebert, A. Perlov, A. N. Yaresko, V. N. Antonov, and S. Uba, to be published.

[70] C. Kittel, *Phys. Rev.* **83**, A208 (1951).

[71] G. H. O. Daalderop, P. J. Kelly, and M. F. H. Schuurmans, *Phys. Rev. B* **41**, 11919 (1990).

[72] D. J. Singh, *Planewaves, Pseudopotentials and the LAPW method*, Kluwer Acad. Publ., Norwell 1994.

- [73] G. H. O. Daalderop, *Magnetic Anisotropy from First Principles*, Proefschrift, Delft (1991).
- [74] D. Singh, Phys. Rev. B **43**, 6388 (1991).
- [75] U. Pustogowa, W. Hübner, and K. H. Bennemann, Surf. Sci. **307-309**, 1129 (1994).
- [76] D. S. Wang, R. Wu, and A. J. Freeman, Phys. Rev. Lett. **70**, 869 (1993).
- [77] J. G. Gay and R. Richter, Phys. Rev. Lett. **56**, 2728 (1986).
- [78] M. S. Hybertsen and S. G. Louie, Phys. Rev. B **34**, 2920 (1986).
- [79] Courtesy of U. Pustogowa.
- [80] J. P. Perdew, J. A. Chevary, S. H. Vosko, K. A. Jackson, M. R. Pedersen, D. J. Singh, and C. Fiolhais, Phys. Rev. B **46**, 6671 (1992).
- [81] J. P. Perdew and Y. Wang, Phys. Rev. B **45**, 13244 (1992).
- [82] In general the fcc density of states is much more structured and asymmetric than the bcc density of states.

FIGURES

FIG. 1. Geometry of the different layers investigated in this paper. The twodimensional unit cell containing one atom is shown, deduced from the fcc lattice in the (110), (001) and (111) direction.

FIG. 2. Chains built by stretching the Fe(111) monolayer as indicated. The unit cell used for the bandstructure calculation is indicated by the solid rectangle. To simulate the chains the distance d is increased compared to h . In the case of $d = h$ the layer is equal to the Fe(111) monolayer.

FIG. 3. NOLIMOKE spectra of Fe(001) monolayers with the lattice constant varying from $a = 2.4 \text{ \AA}$ to $a = 2.76 \text{ \AA}$.

FIG. 4. Magnetic moments and spin-orbit coupling constants for Fe(001) monolayers as a function of the lattice constant. $\lambda_{uu}^{l=2}$ up and $\lambda_{uu}^{l=2}$ dn denote the SOC-constants obtained from the matrixelements within the spin-combinations $\uparrow\uparrow$ and $\downarrow\downarrow$.

FIG. 5. Square of the radial function $u_2(r)$ and integrand $u_2(r)^2 \cdot dV/dr$ as a function of the radius. In both cases the highest values are normalized to unity. The scale of the y-axes in the insets are equal, which indicates that changes in the integrand are directly caused by the radial functions.

FIG. 6. NOLIMOKE spectra in the case of a Fe(001) monolayer obtained by Pustogowa *et al.* [75] using an FP-LMTO code and by the present authors using the FLAPW method.

FIG. 7. Comparison of the NOLIMOKE spectra of a Fe(001) monolayer, obtained by using GGA [76], LSDA with the parameterization of [77].

FIG. 8. Comparison of the NOLIMOKE spectra obtained for the Fe(110) monolayer without spin-orbit coupling and with band shifts induced by SOC. The effect of SOC in the wavefunctions via the optical dipole matrix elements has not been taken into consideration.

FIG. 9. NOLIMOKE spectra as a function of the photon energy of the fundamental light for Fe(001), Fe(110) and Fe(111) monolayers using the Cu fcc lattice constant $a=2.56 \text{ \AA}$.

FIG. 10. NOLIMOKE spectra as a function of the photon energy of the fundamental light for Fe(001), Fe(110) and Fe(111) monolayers using the lattice constant $a=2.4 \text{ \AA}$.

FIG. 11. Magnetic moments and spin-orbit coupling constants $\lambda_{uu}^{l=2}$ for the spin-combinations $\uparrow\uparrow$ and $\downarrow\downarrow$ of the Fe(110), Fe(001) and Fe(111) monolayers with the nearest-neighbor distance of Cu fcc bulk $a = 2.56 \text{ \AA}$. The values are plotted as a function of the coordination.

FIG. 12. Magnetic moments and spin-orbit coupling constants $\lambda_{uu}^{l=2}$ for the spin-combinations $\uparrow\uparrow$ and $\downarrow\downarrow$ of the Fe(110), Fe(001) and Fe(111) monolayers with the nearest-neighbor distance $a = 2.4 \text{ \AA}$. The values are plotted as a function of the coordination.

FIG. 13. NOLIMOKE spectrum of the different stripe structures for distances between the stripes varying from h to $h + 1.78 \text{ \AA}$ as described in Fig. 2.

FIG. 14. Magnetic moment and spin-orbit coupling constant $\lambda_{uu}^{l=2}$ for the spin-combinations $\uparrow\uparrow$ and $\downarrow\downarrow$ for the different stripe structures as a function of their “interstripe” distance d .

Fe (110) Fe (001) Fe (111)

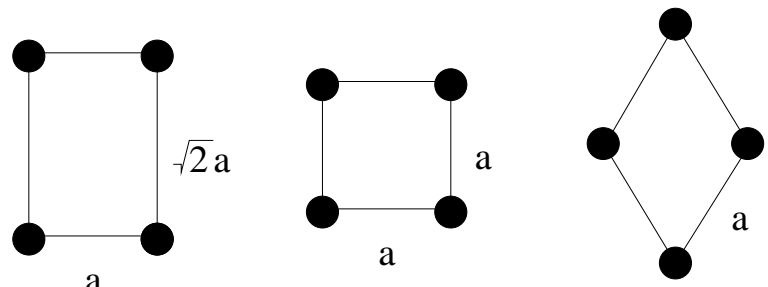


Fig.1

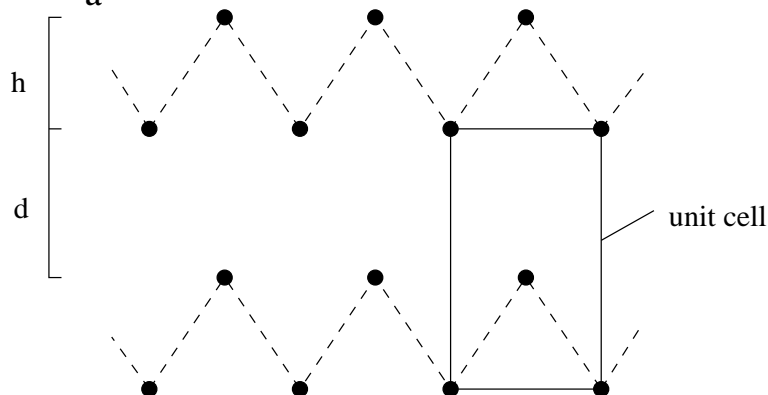


Fig.2

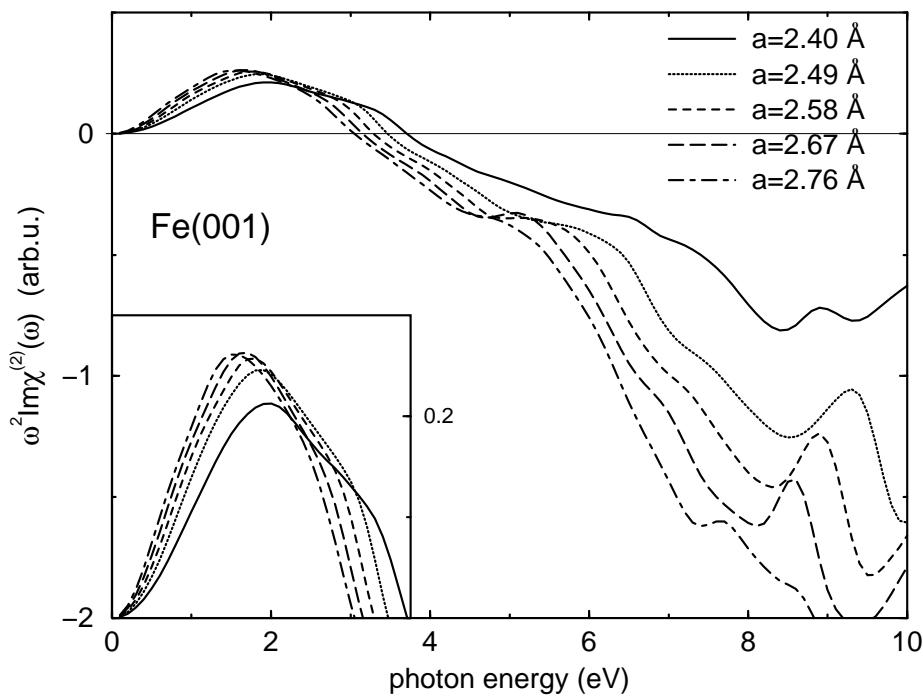


Fig.3

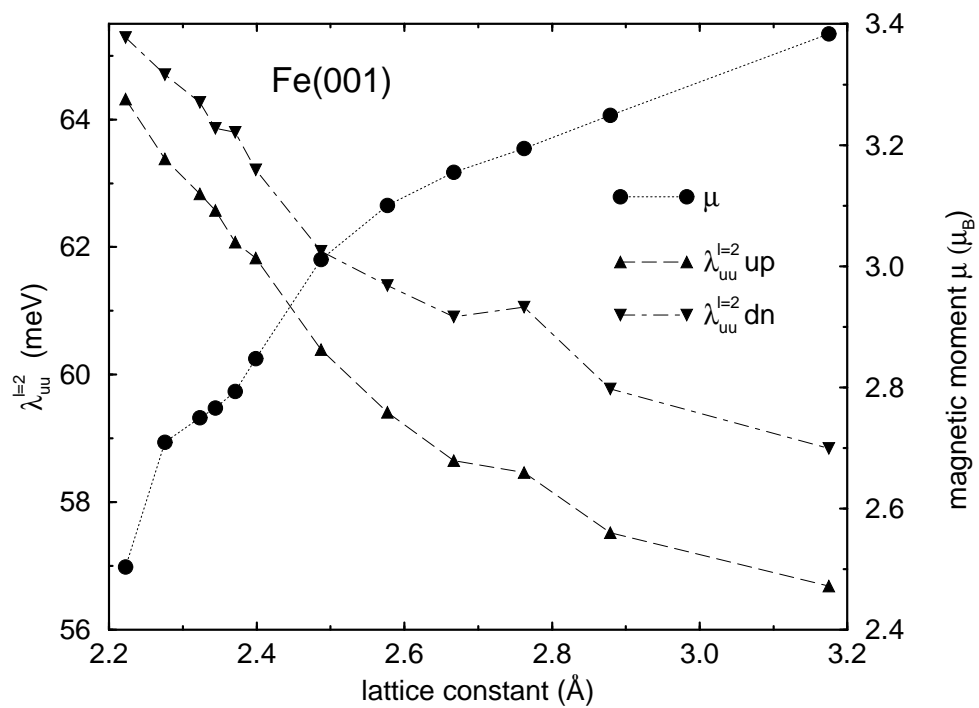


Fig.4

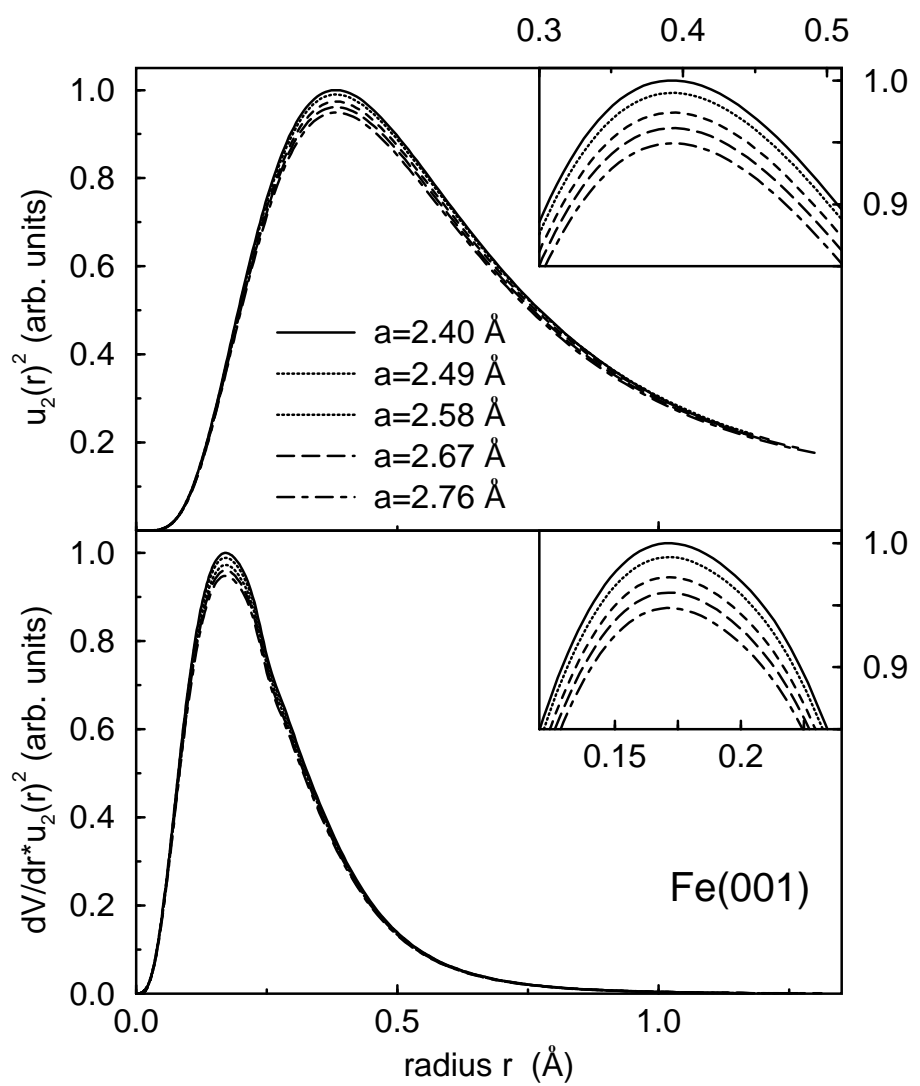


Fig.5

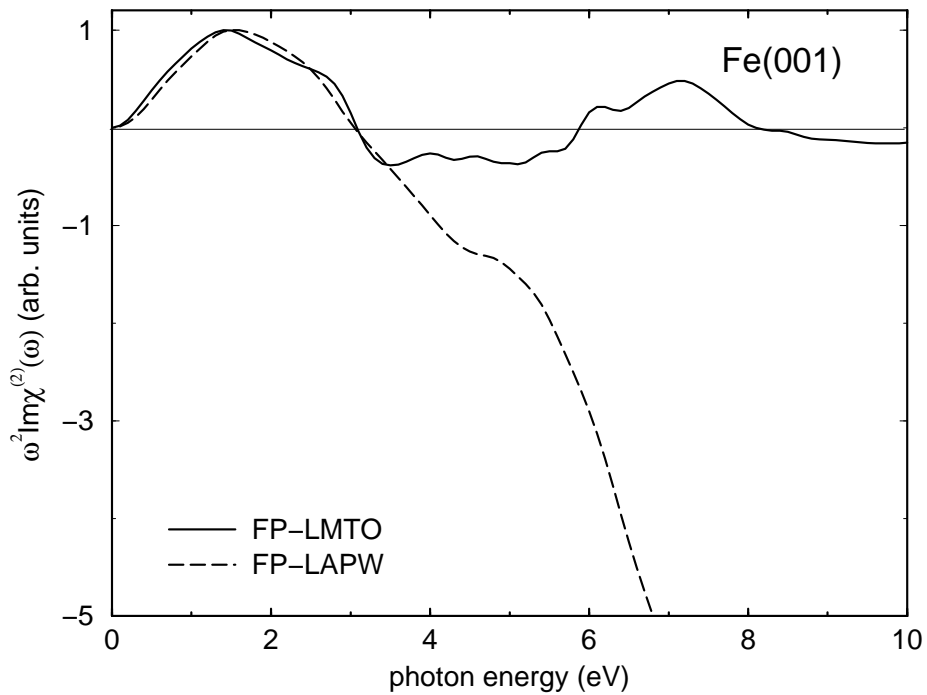


Fig.6

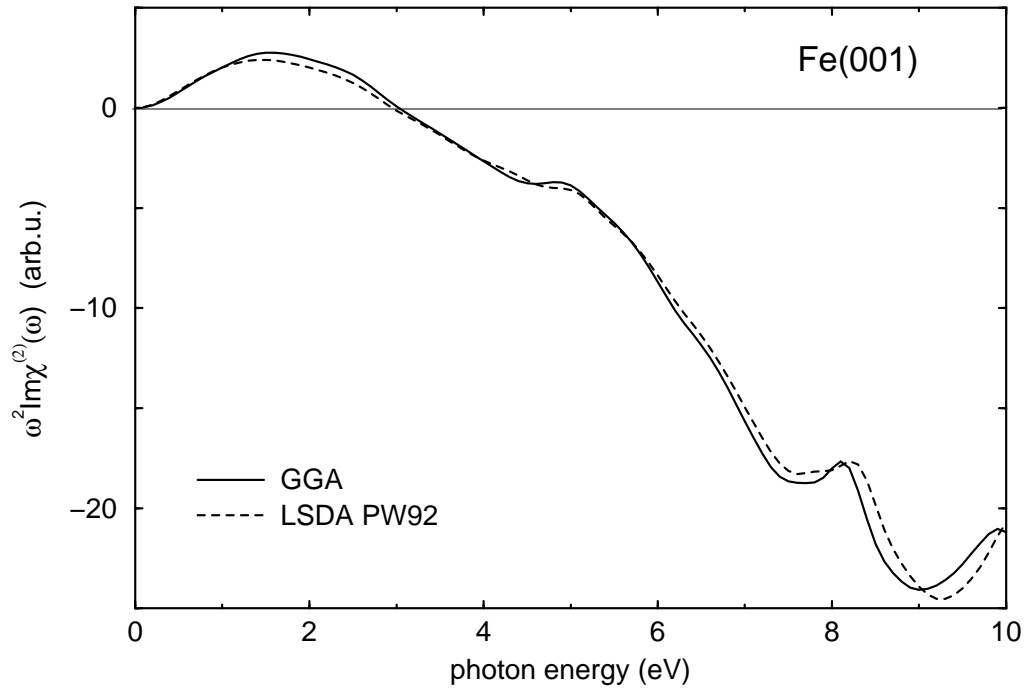


Fig.7

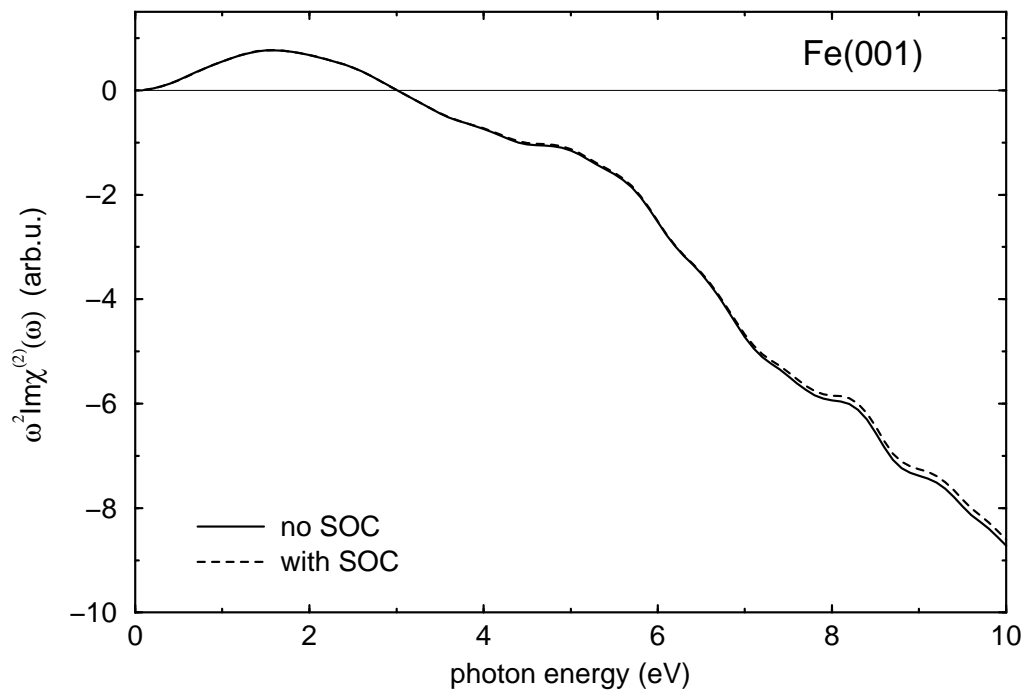


Fig.8

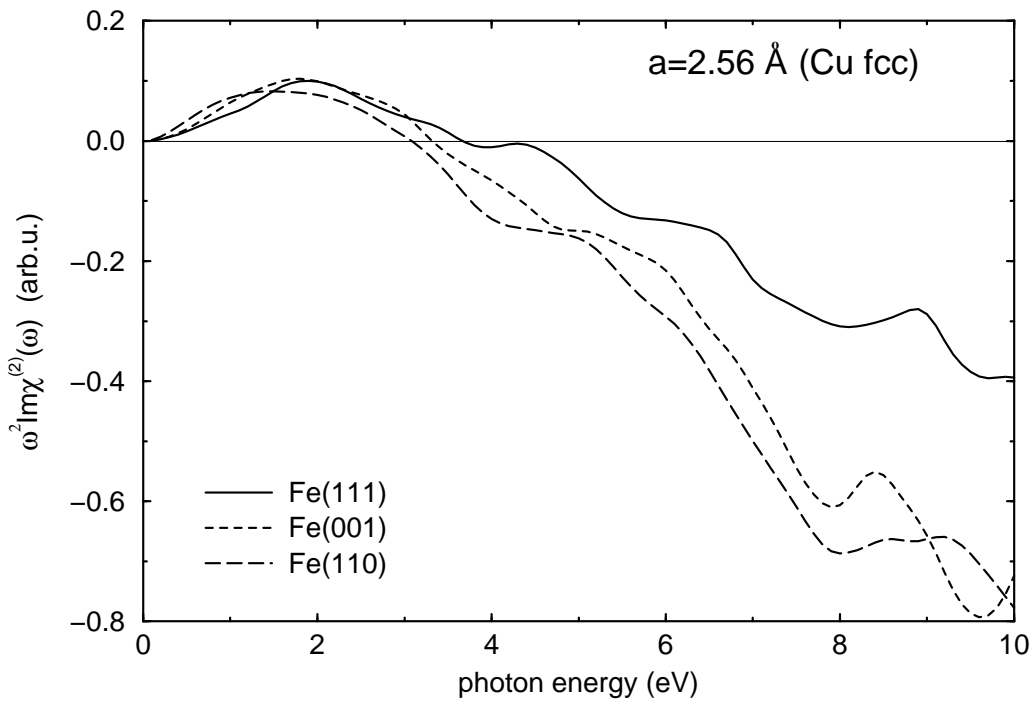


Fig.9

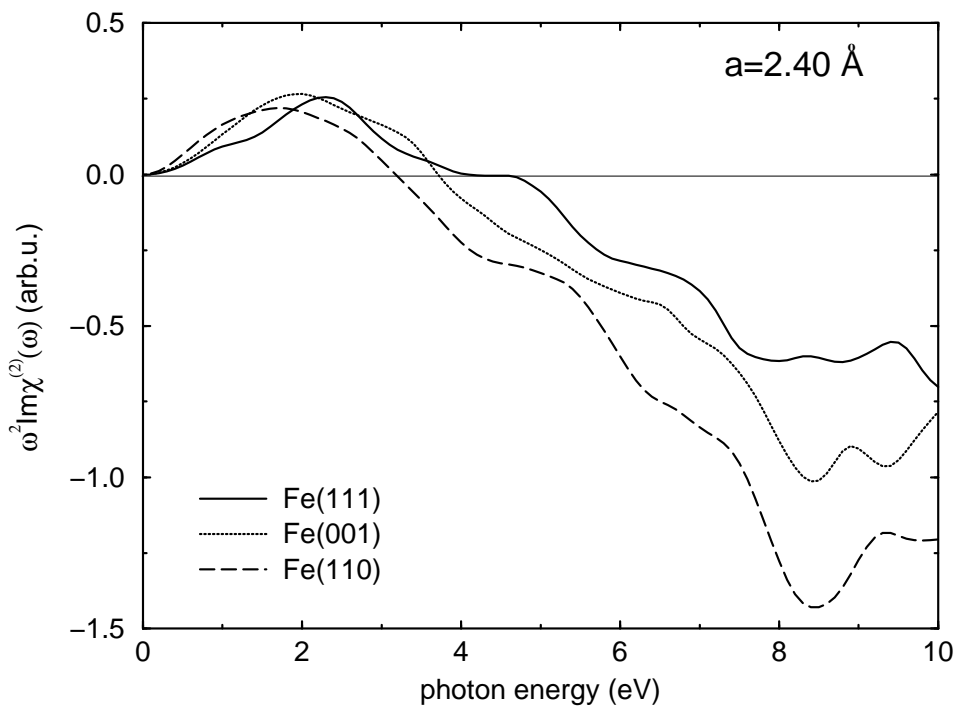
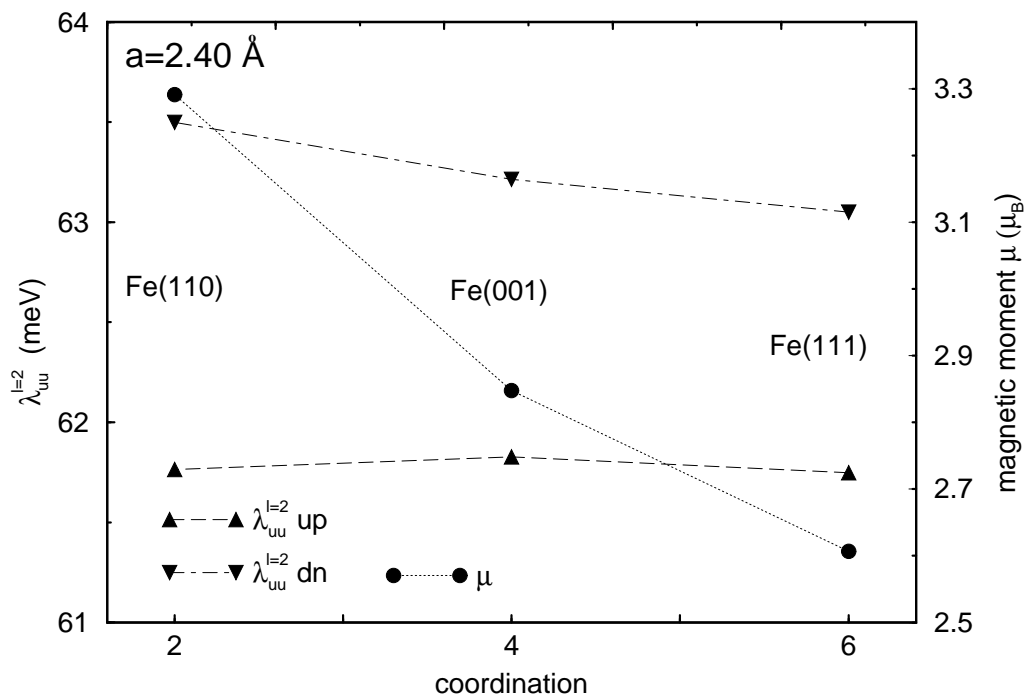
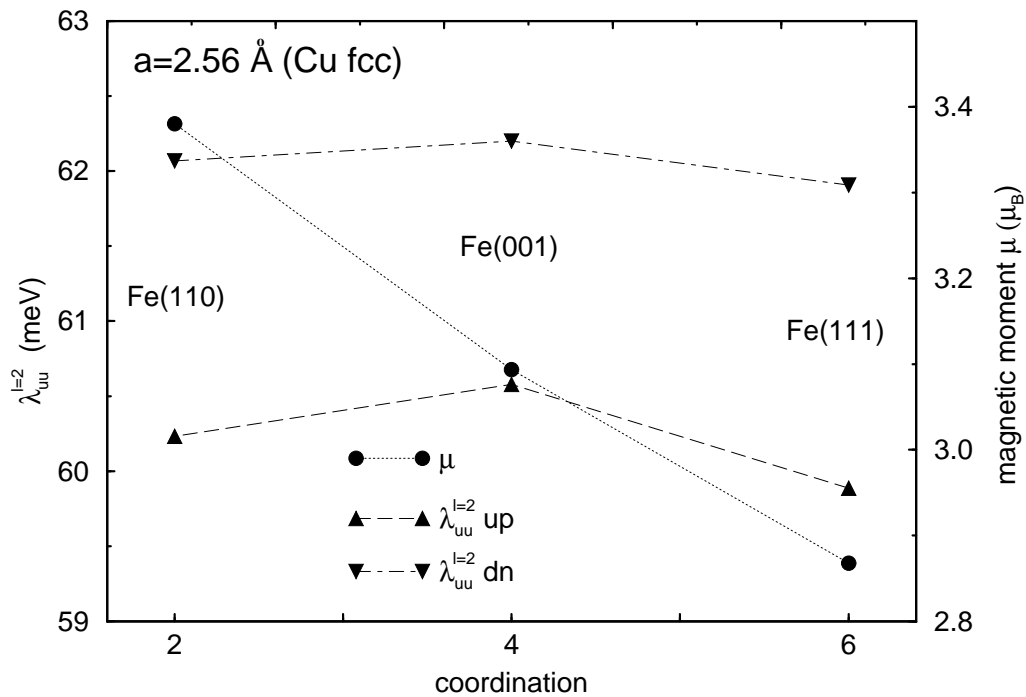


Fig.10



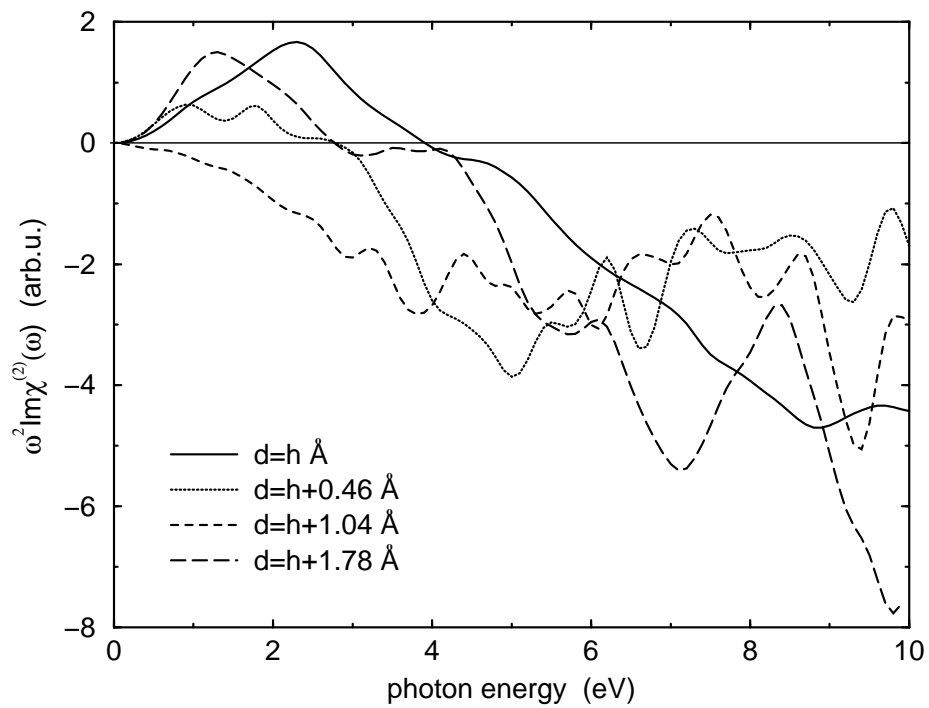


Fig.13

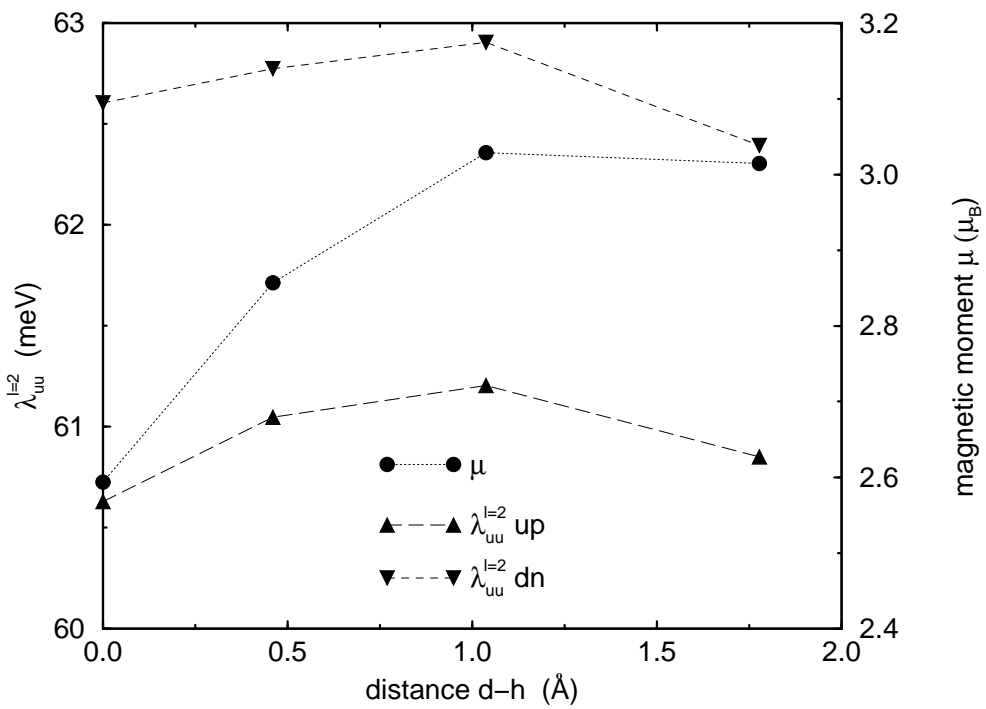


Fig.14

TABLES

TABLE I. Values of the spin-orbit coupling constants λ_{uu}^l and $\lambda_{\dot{u}\dot{u}}^l$ with $l = 1, 2$ for $\uparrow\uparrow$ and $\downarrow\downarrow$ spin-combinations for the Fe(001) monolayer as a function of the lattice constants a between 2.4 and 2.76 Å.

TABLE II. Values of the spin-orbit coupling constants λ_{uu}^l and $\lambda_{\dot{u}\dot{u}}^l$ with $l = 1, 2$ for $\uparrow\uparrow$ and $\downarrow\downarrow$ spin-combinations for the Fe(111), Fe(001) and Fe(110) monolayer with the Cu fcc bulk nearest-neighbor distance $a = 2.56$ Å.

TABLE III. Values of the spin-orbit coupling constants λ_{uu}^l and $\lambda_{\dot{u}\dot{u}}^l$ with $l = 1, 2$ for $\uparrow\uparrow$ and $\downarrow\downarrow$ spin-combinations for the Fe(111), Fe(001) and Fe(110) monolayer with the nearest-neighbor distance $a = 2.4$ Å.

TABLE IV. Values for the spin-orbit coupling constants λ_{uu}^l and $\lambda_{\dot{u}\dot{u}}^l$ with $l = 1, 2$ for $\uparrow\uparrow$ and $\downarrow\downarrow$ spin-combinations of the stripe structures as a function of the “interstripe” distance d .

Tab. 1

[eV]	$a=2.40 \text{ \AA}$	$a=2.49 \text{ \AA}$	$a=2.58 \text{ \AA}$	$a=2.67 \text{ \AA}$	$a=2.76 \text{ \AA}$
$\lambda_{uu}^{l=1} \uparrow\uparrow$	0.40789	0.33736	0.29471	0.26022	0.29714
$\lambda_{uu}^{l=1} \downarrow\downarrow$	0.41127	0.33583	0.29551	0.26304	0.31008
$\lambda_{uu}^{l=1} \uparrow\uparrow$	0.00082	0.00018	0.00061	0.00128	0.00601
$\lambda_{uu}^{l=1} \downarrow\downarrow$	0.00115	0.00041	0.00102	0.00186	0.00697
$\lambda_{uu}^{l=2} \uparrow\uparrow$	0.06182	0.06039	0.05941	0.05865	0.05909
$\lambda_{uu}^{l=2} \downarrow\downarrow$	0.06321	0.06193	0.06140	0.06091	0.06095
$\lambda_{uu}^{l=2} \uparrow\uparrow$	0.01372	0.01604	0.01868	0.02164	0.02459
$\lambda_{uu}^{l=2} \downarrow\downarrow$	0.01385	0.01621	0.01883	0.02175	0.02489

Tab. 2

[eV]	Fe(111)	Fe(001)	Fe(110)	
$\lambda_{uu}^{l=1} \uparrow\uparrow$	0.34339	0.34822	0.34601	
$\lambda_{uu}^{l=1} \downarrow\downarrow$	0.35045	0.35664	0.35519	
$\lambda_{uu}^{l=1} \uparrow\uparrow$	0.00244	0.00262	0.00252	
$\lambda_{uu}^{l=1} \downarrow\downarrow$	0.00299	0.00322	0.00316	
$\lambda_{uu}^{l=2} \uparrow\uparrow$	0.05989	0.06058	0.06023	
$\lambda_{uu}^{l=2} \downarrow\downarrow$	0.06191	0.06220	0.06207	
$\lambda_{uu}^{l=2} \uparrow\uparrow$	0.01807	0.01784	0.01790	
$\lambda_{uu}^{l=2} \downarrow\downarrow$	0.01818	0.01802	0.01802	

Tab. 3

[eV]	Fe(111)	Fe(001)	Fe(110)	
$\lambda_{uu}^{l=1} \uparrow\uparrow$	0.40746	0.40789	0.40900	
$\lambda_{uu}^{l=1} \downarrow\downarrow$	0.41047	0.41127	0.41360	
$\lambda_{uu}^{l=1} \uparrow\uparrow$	0.00084	0.00082	0.00086	
$\lambda_{uu}^{l=1} \downarrow\downarrow$	0.00114	0.00115	0.00123	
$\lambda_{uu}^{l=2} \uparrow\uparrow$	0.06175	0.06183	0.06176	
$\lambda_{uu}^{l=2} \downarrow\downarrow$	0.06305	0.06321	0.06350	
$\lambda_{uu}^{l=2} \uparrow\uparrow$	0.01380	0.01372	0.01370	
$\lambda_{uu}^{l=2} \downarrow\downarrow$	0.01392	0.01385	0.01378	

Tab. 4

[eV]	$d=h$	$d=h + 0.46 \text{ \AA}$	$d=h + 1.04 \text{ \AA}$	$d=h + 1.78 \text{ \AA}$
$\lambda_{uu}^{l=1} \uparrow\uparrow$	0.35653	0.38331	0.38857	0.38502
$\lambda_{uu}^{l=1} \downarrow\downarrow$	0.35388	0.38784	0.39421	0.39004
$\lambda_{u\dot{u}}^{l=1} \uparrow\uparrow$	0.00008	0.00127	0.00146	0.00130
$\lambda_{u\dot{u}}^{l=1} \downarrow\downarrow$	0.00022	0.00166	0.00189	0.00171
$\lambda_{uu}^{l=2} \uparrow\uparrow$	0.06063	0.06105	0.06120	0.06085
$\lambda_{uu}^{l=2} \downarrow\downarrow$	0.06261	0.06277	0.06290	0.06239
$\lambda_{u\dot{u}}^{l=2} \uparrow\uparrow$	0.01518	0.01507	0.01502	0.01504
$\lambda_{u\dot{u}}^{l=2} \downarrow\downarrow$	0.01523	0.01519	0.01514	0.01519q